Modelling and experimental validation of microstructure evolution during the cooling stage of homogenization heat treatment of Al-Mg-Si alloys

Qiang Du , Lina Jia , Kai Tang , Bjørn Holmedal

PII: S2589-1529(18)30124-8
DOI: https://doi.org/10.1016/j.mtla.2018.09.012
Reference: MTLA 105

To appear in: *Materialia*

Received date: 29 May 2018
Revised date: 12 September 2018
Accepted date: 12 September 2018

Please cite this article as: Qiang Du , Lina Jia , Kai Tang , Bjørn Holmedal , Modelling and experimental validation of microstructure evolution during the cooling stage of homogenization heat treatment of Al-Mg-Si alloys, *Materialia* (2018), doi: https://doi.org/10.1016/j.mtla.2018.09.012

Modelling and experimental validation of microstructure evolution during the cooling stage of homogenization heat treatment of Al-Mg-Si alloys

Qiang Du[1], Lina Jia[1,2,3], Kai Tang[1], Bjørn Holmedal[3]

[1]SINTEF Materials and Chemistry, 7465, Trondheim, Norway

[2]Beihang University, 100191, Beijing, China

[3]Norwegian University of Science and Technology, 7491 Trondheim, Norway

Abstract

A CALPHAD-coupled multi-component multi-phase Kampmann-Wagner Numerical modelling framework has been adapted and coupled with a homogenization model to predict the competitive nucleation and growth of multi-sized metastable/stable phase particles during the cooling stage of a homogenization heat treatment. The reported model is the continuation of our previous work on the homogenization soaking modelling [Du et al, Acta Materialia 61 (2013) 4961–4973]. It takes the experimentally verified soaking modelling prediction results as the initial microstructural status and predicts the microstructural evolution during the very last step of the homogenization treatment, i.e. the final cooling process. The model has been applied to two Al-Mg-Si alloys: AA6061 and AA6082. The simulation shows a multi-modal MgSi particle size distribution forms due to multiple nucleation events. For the AA6082 alloy the multiple nucleation events occur mainly due to the local micro-chemistry variations along a dendrite while for AA6061 it is due to the two opposite contributions to supersaturation: the positive contribution by the cooling and the negative contribution by the particles' growth. The interaction of intergranular and intragranular MgSi containing particles have been captured, and the partitioning of Mg and Si solutes among the two different sized MgSi particles has been predicted. The model predictions are in reasonable agreement with the microstructure characterization results obtained with Scanning Electron Microscopy (SEM), Transmission Electron Microscopy (TEM) and Electrical Resistivity Measurement on the quenched samples from some dedicated laboratory-scale homogenization heat treatment experiments. It is concluded that the extended KWN modelling framework is applicable to predict the microstructure evolution during the non-isothermal heat treatment of

multicomponent aluminium alloys.

1. Introduction

Each fabrication step of major metallic structural materials, i.e., aluminium alloys and steels, includes an isothermal process and non-isothermal process such as cooling or heating with or without deformation. It has been well documented that many interesting and industrially critical microstructure evolution phenomena occur during the isothermal processes. For example, during the soaking step of homogenization process of Al-Mg-Si, or AA6xxx alloys, the interdendritic network of the plate-like β-AlFeSi particles transform to the more rounded discrete α-AlFeSi particle, and micorsegration is alleviated making the billets easier to deform plastically [1, 2]. Another example is the precipitation sequence during the ageing such as the one revealed in 6xxx alloys, i.e., starting with Super Saturated Solid Solution (SSSS) and passing several metastable phases (atomic clusters, Guinier-Preston (GP) zones, β" and β'/B') and terminating with Mg_2Si under over-aged conditions [3-8]. On the other side, it also has been recognized that the non-isothermal processes such as cooling and heating have an equally important impact on microstructure evolutions and the final product properties [9-12].

It should be noted that the studies of a non-isothermal precipitation process are also relevant to quenching. Quenching is a critical step before ageing treatment. It is also a non-isothermal process with an extremely high cooling rate. Taking aluminium alloys as examples, quenching involves not only the generation of the quenched-in vacancies, but also precipitation of particles. In their study of quench sensitivity of Al-Mg-Si alloys over a wide range of cooling rate of $3\text{-}120\times10^4$ °C/h, Milkereit and Starink have found from their Differential Scanning Calorimetry (DSC) measurement both of high temperature (typically 500 °C down to 380 °C) and a low temperature precipitation (380 °C down to 250 °C) [13]. Nonetheless, the research efforts dedicated to the non-isothermal process is relatively less than those to the isothermal process.

It is the goal of this paper to revisit this important topic and exploit how a modelling tool, combined with lab-scale experiments, could help in predicting the microstructure evolution

during a non-isothermal process. We will take the cooling process of a homogenization treatment of Al-Mg-Si alloys as an example due to the following two reasons. The first reason is that for the selected alloy system rich and unique microstructure features could be generated by tuning of cooling rate, alloy chemistry and even the initial as-cast microstructure. One can mention the multi metastable phases precipitation and its gradual transformation to more stable phases within the precipitation reaction in Al-Mg-Si alloys. This is unique in reference to the well-studied non-isothermal phase transformation in steels [14] [15] [16]. The co-existence of different sized particles is worthy of noting. The particles' sizes range from several nanometres to several microns, and they often interact with each other leading to the formation of microstructural features such as Precipitate Free Zone (PFZ) [17]. Therefore, this competitive precipitation of various metastable/stable and different sized particles in the Al-Mg-Si is a good case for testing the predictive power of the proposed microstructure model. The second reason is its industrial relevance. As pointed out in [18, 19] [20], for AA6xxx alloys, the cooling has to be designed to re-precipitate as many MgSi particles as possible, in a form and size easily re-dissolvable during subsequent processing for high formability and surface quality. This delicate requirement on microstructure could only be met in a timely manner by the modeling aided alloy design and processing parameter optimization.

Some valuable experimental studies on this interesting non-isothermal precipitation process have been reported. Zajac and Stanislaw have investigated the influence of cooling after homogenization on extrudability and final properties of AA6063 and AA6082 alloys [1]. They have shown that Mg_2Si particles precipitate readily during cooling after homogenization. Above 400 °C, cubic Mg_2Si phase (β phase) precipitates, and below 400 °C only metastable β' phase nucleates predominately on Mn-rich dispersoids. The proportion of β and β' particles depends on the cooling processing parameters. They did not characterize the particle size distribution, but presumably the β and β' particles would exhibit different sizes. They concluded that billets with the β' particles formed at the lower temperature give low flow stress at extrusion temperature, allowing ease deformation and quick particle re-dissolution. Birol has carried out a series of experimental work to study the effects of cooling rates on the

precipitation during the cooling step in 6xxx aluminum alloys [20-24]. His results showed that different density, type and sized precipitates are produced for an alloy cooled at different rates. He also demonstrated that the final microstructure is alloy composition dependent. In general, the amount of both β and β' particles increase with decreasing cooling rates and the content of alloying components [22]. He recommended a homogenization practice with a 6 hours soak at 580 °C followed by step-cooling at 250-300 °C for an AA6063 alloy [20]. He concluded that step-cooling gives a more complete depletion of the aluminum solid solution with the formation of fine, metastable β' particles instead of those coarse and stable Mg_2Si particles [20].

There are also some dedicated microstructure modeling activities towards the homogenization and/or cooling for aluminum alloys. Myhr and Grong have developed a valuable framework for modelling concurrent nucleation, growth and coarsening process and applied it to predict the microstructure evolution during up-quenching and linear heating of age hardening Al-Mg-Si alloys [10]. Myhr and Grong's modeling framework is inspiring and seminal while the model can still be improved toward industrial application by extending it to multi-component alloys. Milkereit and Starink proposed a model for predicting quench sensitivity of heat-treatable Al alloys within the age hardening heat treatment procedure, in which the importance of incorporating reliable thermodynamic and kinetic models have been emphasized [13]. Their model is concise but requires tuning of some non-directly-measurable input parameters. Sun et al [25] have employed a binary Kampamann Wagner Numerical model to predict the precipitation kinetics of Mg_2Si particles, and predicted a bimodal particle size distribution formed during the cooling of homogenization heat treatment. However, their model only considered the precipitation of the stable phase (β phase) and ignored the formation of the metastable β' phase. The most recent study on this interesting topic is due to Priya, Johnson and Krane [26], and they have presented numerical study of microstructural evolution during homogenization heat treatment of Al-Si-Mg-Fe-Mn alloys. However, their model again is only for binary alloys, and they did not consider the precipitation of metastable phases.

It is worthy of noting that the bimodal or multimodal size distribution of single-phase particles has been well investigated in Ni-based alloys due to its important property consequences. Phase field [27] and mean field approach [28] have been adopted to model this interesting microstructural evolution. Whether this bimodal particle size distribution exists in Al alloys is an interesting question that remains to be confirmed. In this paper, we will investigate the microstructure evolution during the cooling stage of homogenization heat treatment of Al-Mg-Si alloys by a combination of modeling and experimental approaches. The employed modeling approach is the CALculation PHAse Diagram (CALPHA)-coupled multi-component multi-phase Kampmann-Wagner numerical (KWN) approach reported by Du and his co-authors in a series of publications [17, 29-33]. The model predictions on the isothermal homogenization soaking and ageing heat treatment of Al alloys had been validated by the experimental microstructure characterizations. In this paper the KWN model will be integrated with the Scheil additivity rule to extend its application to a cooling (non-isothermal) process.

Our justification to select the KWN approach for the homogenization cooling modeling is that the approach is amenable to couple with phase diagrams, numerically robust and efficient, which is advantageous in comparison to phase field method for the applications involved industrial alloys and processes. Although there are more assumptions in the KWN approach than in phase field method such as local equilibrium at the precipitate-matrix interface and the growth is purely diffusion controlled, the KWN approach, when tuned with some key experimental microstructure characterization results, is considered as a suitable modeling tool in investigating industrial alloys' microstructure evolution.

This paper starts with a brief description of the employed modeling and experimental approaches. Then the predictions of the competitive nucleation and growth of β particles and β' particles during a homogenization cooling process are presented. The model predictions are examined in the light of microstructure characterization results carried out with Scanning Electron Microscopy, Transmission Electron Microscopy and Electrical Resistivity Measurement on the samples from some dedicated laboratory-scale homogenization heat

treatment experiments.

2. The microstructural model for the homogenization cooling

The industrial Al-Mg-Si alloy homogenization treatment is often conducted at a temperature as high as possible without causing incipient melting for a couple of hours. This high temperature soaking results in that Mg and Si solutes are taken back into the Al solid solution phase and ready to re-precipitate intra-granularly and inter-granularly upon cooling. Given insufficient soaking time or low soaking temperature, the spatial distributions of the alloying components might remain non-uniform across a secondary dendrite arm, i.e., the local micro-chemistry varies leading to different kinetic response during the cooling. In addition, constituent particles, which initially were formed at the end of solidification (casting process) in the interdendritic region, would also grow and drain some solute atoms reducing the total solute supersaturation available for the intragranular MgSi particles formation during the cooling. These are the unique features which have motivated us to perform the research activities reported in this paper.

To describe the complex homogenization, precipitation and their interactions process, some adaptions to the modeling framework reported recently by the authors in [17, 29, 30, 33] need to be made. These adaptions are described in the following three subsections.

2.1 Modeling precipitation during a non-isothermal process

The precipitation process is modeled by adapting the multi-component multi-phase Kampmann-Wagner Numerical framework described in [33]. Below only a summary of the KWN approach is given, and the focus is on its adaption.

The KWN approach is built on the classical nucleation, growth and coarsening laws, and the particles interactions are handled via the mean filed concept. The essence of this framework is that precipitate size distribution curve could be subdivided into size classes, each of which is associated with some identical precipitates. The temporal evolution of the size distribution is

then tracked by following the size evolution of each discrete size class.

The extension to the KWN framework toward the cooling process is the calculation of nucleation incubation time during a non-isothermal process. The Scheil additivity rule [34] is adopted for this extension. The rule states that the fractional nucleation time are additive, and that nucleation begins when the sum of such fractional nucleation time attains the value of unity. The criteria for nucleation can be expressed as

$$\sum_{i=1}^{n} \frac{\Delta t_i}{\tau_i} = 1 \qquad \text{(Eq.1)}$$

Where Δt_i is the time of isothermal held at temperature T_i, and τ_i the incubation period. There is a re-visit to this rule very recently owing to its important role in bridging the gap between isothermal and non-isothermal transformations [35]. It has been accepted that the reactions for which the additive rule is justified are called isokinetic, implying that the fraction transform at any temperature depends only on time and a single function of temperature. This rule fits well within the context of the KWN modelling framework.

2.2 The non-homogenization process

Even soaking can homogenize the solute spatial distribution across a dendrite arm, the subsequent cooling would cause variations in local microchemistry, and this cooling-induced "non-homogenization" process needs to be tracked to predict the final microstructure.

The first microstructural response to the cooling is growth of constituent particles, which would drain solutes gradually from their adjacent dendrite arms. The extent of this draining at the dendrite centre is least due to their longest diffusion distance to these constituent particles. The second response to the cooling is precipitation, and the precipitation model is described in the previous subsection. However, it is worthy of noting that precipitation kinetics might vary from the centre to the periphery of a dendrite arm due to its local microchemistry variation. As to be shown later, this local microchemistry variation is responsible for the multi-modality in particles size distribution curves. On the other hand, precipitation would reduce the local solid solution solute level, therefore affect the solute diffusion along the

dendrite arm.

This non-homogenization process is modelled by adapting the framework we reported earlier in [17]. The original model consists of a 1D Finite Volume Method for solving the diffusion along a half "average" dendrite arm, and the applications of the KWN model to each volume element for predicting precipitates nucleation and growth. On the base of the original framework two adaptions have been made to enable modelling the cooling process. The first adaption is to extend the original assumption that thermodynamic equilibrium is held in interdendritic region from the soaking stage to the cooling process. This extension is justifiable as the same assumption has been validated in the heating stage of a homogenization heat treatment [17]. The second adaption is to turn on the nucleation model for MgSi containing particles during the cooling.

2.3 Initial microstructural status and some thermo-physical input parameters of the cooling simulations

The initial microstructural status, to be subjected to cooling, results from alloy chemistry, casting conditions and homogenization soaking treatment parameters. This initial microstructural status is as important as the cooling rate in determining the final microstructure status. In our simulation, the initial microstructure state is predicted with the comprehensive and experimentally validated homogenization soaking modeling framework for 6xxx alloys [36, 37]. Some experimental data have been used confirming the model predictions while the focus of this paper is on the cooling process.

The application of the KWN model to the cooling process involves the tuning of the nucleation model input parameters: interfacial energies and number of heterogeneous nucleation sites. The interfacial energies have been evaluated in [33] by employing the solution enthalpy method proposed in [38] and their Al-Mg-Si thermodynamic CALPHAD database [39]. They are listed in Table 1 for all the involved metastable and stable phases, i.e. β' and β. However, these calculated values can only be used as guidance in tuning the values.

Some key experimental measurement data on incubation times must be used for the final tuning. The number of heterogeneous nucleation sites is chosen as $0.03\times10^{18}m^{-3}$ and $2.6\times10^{18}m^{-3}$ for the AA6061 and AA6082 alloys respectively according to the experimental TEM characterization performed in our research (to be reported in Section 4). It should be acknowledged that the tuning of these nucleation model input parameters is restricting the applications of the precipitation kinetics modeling approach. Nevertheless, numerical simulation is still considered to be valuable due to the reduction of the times of experimenting.

The other thermo-physical input parameters include thermodynamic databases and diffusivities. The thermodynamic description of the metastable phases in the Al-Mg-Si alloys, established with first-principles total energies and frozen phonon calculations and verified with experimental measurements by Povoden-Karadeniz et al in [39], is adopted to calculate solvus temperature and partition coefficient used in all the simulations performed in this paper. The diffusivity of the alloying component Mg and Si are taken from the work of Du et al [40]. These parameters are listed in Table 2.

3. Experiments

3.1 Materials and lab-scale cooling experiments

The initial materials were DC cast AA6082 and AA6061 billets. The chemistry of the alloys is listed in Table 3.

The lab-scale homogenization heat treatment of the two Al alloys were conducted in a programmable furnace. The heat treatment of AA6061 consists of heating from room temperature to 580 °C at a rate of 200°C/hour, soaking for up to up to 20 hours and cooling down at the rate of 125°C/hour*. The heat treatment of the AA6082 alloy consists of a heating of 200℃/hour from room temperature and soaking at 560℃ for 2 hours and cooling down at

* The reported cooling rate is the average between the soaking temperature and 250 °C.

the rate of 150℃/hour. A schematic drawing of the thermal history is shown in Fig. 1, and the microstructure characterization samples are taken out of the furnace at the end of soaking, 550 ℃, 500 ℃, 450 ℃,400 ℃, 350 ℃, 300 ℃, 250 ℃, 200℃ respectively for quenching in water.

It shall be pointed out that in addition to their industrial relevance the selections of the two alloys' compositions and their corresponding heat treatment parameters are based on the following two criterions:

1. In AA6061, it is expected that after soaking treatment almost no constituent particles remain, and fully homogenized and particle free solid solution phase is obtained. Therefore, spatial microstructural inhomogeneity can be neglected, and the only microstructural evolution to be simulated is the precipitation of intragranular particles. The simulation performed for this alloy is named "single cell simulation" in this paper.
2. In AA6082, plenty of constituent particles and spatial microstructural inhomogeneity exists during the cooling. Therefore, the simulation domain is a 1D domain starting from the center of the dendrite to its periphery and consisting of 10 finite volumes. The solute diffusion equation for Mg and Si solute are solved in this 1D domain. The different nucleation and growth kinetics of MgSi particles in each finite volume are tracked with the extended KWN model. The simulation performed for this alloy is named "full simulation" in this paper.

3.2 Experimental characterization techniques

A set of experimental microstructural characterization techniques including Scanning Electron Microscopy (SEM), Transmission Electron Microscopy (TEM) and electrical resistivity measurement have been used to characterize the water quenched samples.

The microstructural characterization of large particles was determined from SEM images taken with a Hitachi S-3000N SEM. An accelerating voltage of 20 keV for the electron beam and working distance of 15 mm were adopted. SEM micrographs were collected in back-scattered imaging mode. Quantitative measurements of the constituent particle fraction

were made from more than 20 pieces of 180μm×100μm SEM micrographs.

Thin foils for TEM characterization of tiny MgSi particles were prepared by a conventional method, i.e. the disks with a thickness of about 2mm were cut, mechanically ground down to 50~70 μm. Disks with a diameter of 3 mm were further electro-polished to TEM specimens with a Struers TenuPol-5, using a solution of 1/3 nitric acid and 2/3 methanol. The applied voltage was 20V at a temperature of -25℃.

Electrical resistivity measurements were used to follow the overall average compositional changes during the cooling. Measurements were made using a Sigmatest® 2.069 (Foerster Instruments Inc.) with an 8 mm probe using a measurement frequency of 60 kHz.

4. Results and discussion

The predictions by the proposed model on the microstructural evolution during the cooling of the AA6061 and AA6082 alloys and their comparison with the experimental measurement results are reported in this section. We start with the subsection dedicated to the initial microstructural status for the cooling process and simulation set-ups, and then move to the single cell simulation of the AA6061 alloy. In the single cell simulation, the model's capability of capturing the intragranular precipitation kinetics during the cooling is demonstrated and validated. The last subsection is on the full simulation of the AA6082 alloy, and the model ability of capturing the complex microstructure evolution during the cooling is demonstrated and validated.

4.1 The initial microstructural status upon soaking treatment and simulation set-ups

Fig. 2 shows the microstructural states of the AA6082 and AA6061 alloys after the soaking treatment. Light grey Fe- and Mn-bearing interdendritic constituent particles are presented in both of the two alloys; however, their sizes and number density are much higher in AA6082 (Fig. 2a) than in AA6061 (Fig.2c) due to the former's higher alloy contents. Some black particles are present in the AA6082 image and have been identified by EDS analysis as Mg_2Si phase. The decoration of the interdendritc regions by constituent particles also permit the

estimation of secondary arm spacing, which is about 20 μm for the two alloys. In addition to those constituent particles many intragranular tiny grey dispersoids have been found. Their sizes (at the scale of 10 nm as to be shown in the TEM images of Fig. 5 and 9) are not discernable with these SEM images. Fig. 2b reveals that the spatial distribution of these tiny grey dispersoids are non-uniform. They tend to stay away from constituent particles, therefore a PFZ with a thickness of few microns forms in-between dispersoids and constituent particles. While in the AA6061 alloy (Fig. 2d), the number density of dispersoids are very low indicating PFZ has spread to the maximum. These images confirm the two selection criterions listed in Section 3.1 have been satisfied.

In addition to these SEM measurement results numerical simulations with the experimentally validated modeling framework by Liu et al for AA6xxx alloys [36] have been carried out to pin down the detailed initial microstructural status to be used for the subsequent cooling simulations. Fig. 3 presented the predicted profiles of dispersoids fraction along an average dendrite arm (with the half spacing of 10 μm) at the end of soaking. Indeed, due to the relatively low alloy contents, higher soaking temperature (580℃ vs 560℃) and much longer soaking time (20 hours vs 2 hours), the simulations predict that the AA6061 alloy has been fully homogenized and no dispersoids remain while there is about 2μm PFZ in the AA6082 alloy. These predictions agree well with the SEM images presented in Fig. 2

The simulations also predict the dispersoids size distributions, solid solution levels, constituent particles fractions, and some of which are summarized in Table 4. For the AA6082 alloy, the predicted particles fractions agree very well with the measured fractions (by SEM) for Fe-Mn-containing containing particles (1.2%) and Mg_2Si (0.4%) particles as shown in Fig. 4. For AA6061 no Mg_2Si but few Fe and Mn containing particles have been found in the SEM images. This observation is in agreement with the model predictions.

Fig. 4 shows how the number densities and fractions of interdendritic Fe-Mn-bearing particles and MgSi particles evolve during the cooling. Considering the measurement errors, it is safe to conclude that the Fe-Mn-bearing particles are very stable while significant grows occur to the Mg-Si constituent particles with its number density doubled and fraction more than tripled.

From these experimental and validated simulation results, two assumptions are made in the cooling simulations reported in this paper:

1. The two alloys are assumed to be ternary Al-Mg-Si alloys and the alloying element of Fe and Mn are not included. This is because our research focuses on intragranular and intergranular Mg-Si particles, and Fe and Mn containing particles are inert during the cooling.
2. Due to the lean contents of the AA6061alloy, upon soaking treatment all the Mg_2Si constituent particles have dissolved, and only few Fe and Mn containing particles remain as evidenced by Fig. 2 (c) and (d). Since homogeneous microstructural status has been achieved after soaking treatment, it is feasible to expect precipitation behaviours for any locations (the centre or periphery) of a dendrite are identical. This justifies the "single cell" simulation to be reported in Section 4.2.
3. Due to the high Mg and Si contents in the AA6082 alloy, some intergranular Mg_2Si particles, which were formed at the end of the solidification during casting, have survived the soaking treatment. During the cooling they would continue to grow interfering the nucleation and growth of intragranular Mg-Si particles. Therefore, a full simulation must be carried to treat the diffusional transportation of Mg and Si solute to constituent particles and the different precipitation kinetics at the various locations along a dendrite arm.

The other input parameters to the cooling simulations have been listed in Table 1 and 2.

4.2 The precipitation of intragranular MgSi particles in the AA6061 alloy

The first simulation is for modeling the precipitation of intragranular Mg-Si particles in the AA6061 alloy. As discussed earlier in Section 4.1, the initial microstructural status is the solid solution phase obtained from the soaking simulation. The long-range diffusion and the interference with intergranular particles (i.e. constituent particles) are not included in this single cell simulation. This purpose of the simulation is to demonstrate the model capability of capturing the intragranular precipitation kinetics during the cooling process.

The prediction results are presented in Fig. 5 together with the experimental measurement results. Fig. 5 (a) and (b) are the two typical images showing the particles structures obtained after the cooling. The particles, identified as β' phase, are of needle shape, and the length directions are along one of the three [001] directions. From the TEM images like the ones shown in Fig.5 (a) and (b), statistical data are collected from the total observation volume of about 20 μm^3. An "average" particle occupies a volume of 0.162 μm^3, which corresponds an equivalent spherical particle with the radius of 0.34 μm. Its aspect ratio is 9.8 and volumetric fraction is about 0.5%. These measurement results are in reasonable agreement with their predicted counterparts, which are 0.69% and 0.38 μm respectively.

From these TEM images the particles length and cross section area distribution histogram are obtained, and they are plotted in Fig. 6 (a) and (b) together with the model predictions on particles length distribution histogram. It should be acknowledged that the model prediction was made with the assumption of constant aspect ratio (which is equal to 4.0) for all the particles. It implies that the predicted cross section area histogram and length histogram only differ by a scaling factor (i.e., aspect ratio), and therefore only the predicted histogram on length distribution is plotted (see Fig. 6 (c)). Obviously as shown by the measured area and length histogram in Fig. 6 (a) and (b), although they can be fitted with log-normal distribution functions, they are not self-similar indicating the non-linear relation exists between particles' cross section area and length. This assumption has made the comparison between the measured and predicted histograms very difficult. Another discrepancy is that the predicted histogram, which has a small peak at about 0.64 μm and a large peak at about 2 μm, cannot be fitted with a log-normal distribution function. How to make a reconciliation is a challenge. On the modelling side, the mean field KWN approach has to be improved or modified to generate an asymptotic solution with the form of log-normal distribution density function. Nonetheless if we could ignore the first predicted peak, the measured histogram could be considered in qualitative agreement with the prediction.

4.3 Modelling the local variation in precipitation kinetics along a dendrite arm in the AA6082 alloy

In reference to the AA6061 alloy, the solute contents in the AA6082 alloy are higher, which leads to the survival of some intergranular particles after the 2 hours soaking treatment. As we have discussed in Section 4.1, these particles would drain solute from their adjacent dendrite arms causing spatial variation in microchemistry along a dendrite arm. This local variation in microchemistry is well illustrated by the predicted average composition profiles as shown in Fig. 7. At the start of the cooling, the Mg and Si profiles (the red curves in Fig. 7 (a) and (b)) are very flat from the centre (the left-hand side of the figure) to the periphery of the dendrite (the right-hand side of the figure). Please note the curves do not include the highly solute-enriched inter-dendritic region, which would be at the right-hand side if added. The inter-dendritic region serves as the solute sink during the cooling. As the cooling proceeds to 500℃, the Mg level in the dendrite has decreased from 0.8at% to 0.5at% while Si from 1at% to 0.8at% due to the diffusional transportations to the inter-dendritic regions for the growth of Mg_2Si constituent particles. The differences of the local microchemistry in the centre and the periphery of the dendrite arm is about 0.05at% for both Mg and Si. When temperature drops to 470℃ these differences become 0.07at% and 0.09at% respectively representing about 17% and 15% deviations from the average solute solution levels. These deviations give the advantages for nucleation and growth in the centre of the dendrite leading to microstructural heterogeneity as to be reported in this section.

4.3.1 The interactions between the intragranular and intergranular Mg-Si particles

Fig. 8 are the SEM images taken on the samples cooled to room temperature, in which small non-uniformly distributed intragranular white Fe- and Mn-containing dispersoids, black Mg_2Si particles and large Fe and Mn containing constituent particles can be found. In comparison to the initial microstructural status shown in Fig. 2 (a) and (b), there are no obvious changes in the Fe- and Mn-bearing particles, while existing Mg_2Si particles have undergone substantial growth and new Mg_2Si particles have formed. These new Mg_2Si particles could nucleate in either the interdendritic region or a dendrite and grow into as big as

those constituent particles. As we discussed in Section 4.1, these Mg_2Si particles would compete with the intragranular metastable particles for Mg and Si solutes. The intragranular metastable Mg-Si particles, obtained after the cooling of the AA6082 alloy, are too small to be revealed with the SEM imaging. They can be seen under TEM as to be shown in Fig. 9 (a) and (b). They, nucleated on the Fe and Mn containing dispersoids, are identified as β' phase and of needle shape, and their longitudinal directions are along one of the three [001] directions.

The model's predictions and experimental measurements on the big and small intragranular Mg-Si particles fraction are presented in Table 5. The measurement of Mg_2Si constituent particles fraction has been performed on many SEM images like the ones shown in Fig. 8 (a) and (b) while the intragranular Mg-Si particles fraction on the TEM images like the ones shown in Fig. 9 (a) and (b). Considering the measurement errors and the difficulties in distinguishing between the intragranular and intergranular Mg_2Si particles, the agreement is reasonable, which justify the treatment of long-range diffusion (along the dendrite arm) and short-range diffusion (inter particle distance) in the employed modelling framework.

4.3.2 the multiple nucleation peak and multi-modal particle size distribution

The simulation reveals the significant influences caused by local microchemistry variations on nucleation kinetics. Fig. 10 shows nucleation rates at three selected locations of a dendrite arm, i.e. the periphery, one quarter from the periphery and centre. The very first nucleation peak occurs at the centre of the dendrite when the temperature drops to 469 ℃ due to its highest supersaturation. This is about 10 minutes earlier than the first nucleation peak at the one quarter location, and 40 minutes earlier than the first peak at the centre location. The earlier nucleation gives the particles in the centre location advantages in solute absorption and growing time. They grow into particles with the size of 0.34 μm at the end of cooling, which is larger than the ones with 0.23 μm at the quarter position and 0.046 μm at the centre. The multiple nucleation events resulting from the local micro-chemistry variations along a dendrite is a new origin for the "multi-modality" in the particles size distribution curve. It has not been mentioned in the Ni alloys modelling work reported in Ref [27] and Ref. [28]. Indeed, the reported multi-modality in the Ni alloys results from the two opposite

contributions to supersaturation: the positive contribution by the cooling and the negative contribution by the particles growth. Our finding is of practical values as it implies that to avoid multi-modal particle size distribution it is not enough to tune the cooling rate alone. Soaking or solution heat treatment also needs to be optimized to remove the local micro-chemistry variation.

Each curve in Fig. 10 is divided into β (Mg_2Si) phase nucleation stage and β' phase nucleation stage as indicated by the vertical blue line. The β (Mg_2Si) phase nucleation stage is between 470 °C and 350 °C while β' phase nucleation stage between 325 °C and 275 °C. These multi-nucleation nucleation peak prediction is in qualitative consistency with the one reported by Zajac and Stanislaw on the similar alloys [1]. They also have seen that above 400 °C, cubic Mg_2Si phase (β phase) precipitates, and below 400 °C only metastable β' phase nucleates predominately on Mn-rich dispersoids. It is also noteworthy that there are three nucleation peaks for the centre and periphery location during the β phase nucleation stage. This is due to that the continuous cooling has led to the building up of supersaturation in the matrix phase. If the growth of existing particles is not quick enough to consume the built-up supersaturation, the thermodynamic drive force for nucleation would become larger, and eventually nucleation is re-initiated. This is the same mechanism as the one reported in Ni alloys [27] [28].

From many TEM images like the ones shown in Fig. 9 (a) and (b), statistical data are collected from the total observation volume of about 400 μm^3. The measured particles cross area and length distribution histograms are plotted in Fig. (a) and (b). Unlike the measured histograms for AA6061 presented in Fig. 6 (a) and (b), the histograms in Fig.11 cannot be fitted by any log-normal or normal distribution functions. As a matter of fact, these histograms are of multi-modal nature, which supports the multi-nucleation peak prediction presented in Fig. 9. In this sense these measured histograms validate qualitatively the proposed modelling framework. It should be acknowledged that the quantitative comparison on the particles area/size distributions requires the further extension of the model to handle particle growth anisotropy.

The TEM images also allow the measurement of the volumetric number density of the particles, which is 2.6/μm^3. An "average" particle occupies a volume of 0.0018 μm^3 which corresponds to an equivalent spherical particle with the radius of 75 nm, and its aspect ratio is 8.0. The total volumetric fraction is about 0.47%, which is in reasonable agreement with the model prediction of 0.3%.

Finally, the experimentally measured resistivity evolution curve is compared with the model prediction in Fig. 12. This comparison is made possible by converting the predicted the solid solution solute levels of Mg and Si into the electrical resistivity using Matthiessen's law [41]:

$$\rho = \rho_0^{alloy} + \alpha_{Mg}^{net} \Delta C_{Mg} + \alpha_{Si}^{net} \Delta C_{Si} \qquad \text{(Eq.2)}$$

where ρ_0^{alloy} is the initial (i.e. it includes scattering contributions from (i) temperature, (ii) all the different solutes, including trace additions, and (iii) constituent particles), α_{Mg}^{net} and α_{Si}^{net} are the net resistivity coefficients (i.e. the difference between the contribution of the element in solution and out of solution [41]) for Mg and Si respectively. ΔC_{Mg} and ΔC_{Si} are the predicted changes in Mg and Si solute level during cooling. The values for ρ_0^{alloy} is set to be 37.5 nΩ·m to fit the first experimental measurement value, and α_{Mg}^{net} and α_{Si}^{net} are taken to be 6.2 nΩ·m/wt% and 5.4 nΩ·m/wt% respectively according to [41]. In general, the agreement between the model predictions and the experimental measurements shown in Fig. 12 is satisfactory.

It is worthy of pointing out again that the agreement demonstrated here cannot be achieved without some key experimental input. Firstly, the number of heterogeneous nucleation site is taken from the TEM measurement. Secondly the interfacial energy needs to be tuned and the effect of aspect ratio is considered in an averaging manner. The value of the proposed model lies in reproducing the full temporal microstructural evolution after being given several key experimental measurement data.

5. Conclusions

The microstructural evolution during the cooling process of homogenization heat treatment of two Al-Mg-Si alloys have been predicted by an extended CALPHAD-coupled multi-scale multi-component multi-phase Kampmann-Wagner Numerical modelling framework. For the AA6082 alloy, the predicted Mg-Si particle size distribution is multi-modal resulting from multiple nucleation peaks. The interaction of intergranular and intragranular Mg-Si containing particles have been captured. The model predictions are in good agreement with the microstructure characterization results obtained with SEM, TEM and Electrical Resistivity Measurement on the quenched samples from some dedicated laboratory-scale homogenization heat treatment experiments. It is concluded that having been tuned with several experimental measurements the proposed modelling framework is a valuable tool for the prediction of the microstructure evolution during the non-isothermal heat treatment of multicomponent alloys.

6. Acknowledgements

This research work is the part of the KPN project PRIMAL work package 'Modelling Based Alloy Development' (project number: 236675) financially supported by the Research Council of Norway and the industrial partners, Hydro Aluminum, Aloca Norway.

7. References

1. Zajac Stanislaw, B.B., Jonsson Christer, *Influence of cooling after homogenization and reheating to extrusion on extrudability and final properties of AA6063 and AA6082 alloys.* Materials Science Forum, 2002. **396-402**.
2. Samaras, S.N. and G.N. Haidemenopoulos, *Modelling of microsegregation and homogenization of 6061 extrudable Al-alloy.* Journal of Materials Processing Technology, 2007. **194**(1–3): p. 63-73.
3. Marioara, C.D., et al., *Atomic model for GP-zones in a 6082 Al–Mg–Si system.* Acta Materialia, 2001. **49**(2): p. 321-328.
4. O. Engler; C. Schafer, H.J.B., C.D. Marioara, M. Kozuka, H. Shishido, Y. Aruga, *A Combined TEM and Atom Probe Approach to Analyse the Early Stages of Age Hardening in AA 6016.* Materials Science Forum, 2016. **877**: p. 6.
5. Marioara, C.D., et al., *The influence of temperature and storage time at RT on nucleation of the beta '' phase in a 6082 Al-Mg-Si alloy.* Acta Materialia, 2003. **51**(3): p. 789-796.
6. Marioara, C.D., et al., *The influence of alloy composition on precipitates of the Al-Mg-Si system.* Metallurgical and Materials Transactions a-Physical Metallurgy and Materials Science, 2005. **36A**(3A): p. 691-702.
7. Marioara, C.D., et al., *Post-β'' phases and their influence on microstructure and hardness in 6xxx Al-Mg-Si alloys.* Journal of Materials Science, 2006. **41**(2): p. 471-478.
8. Chen, J.H., et al., *Atomic pillar-based nanoprecipitates strengthen AlMgSi alloys.* Science, 2006. **312**(5772): p. 416-419.
9. Bratland, D.H., et al., *Overview No. 124 Modelling of precipitation reactions in industrial processing.* Acta Materialia, 1997. **45**(1): p. 1-22.
10. Myhr, O.R. and O. Grong, *Modelling of non-isothermal transformations in alloys containing a particle distribution.* Acta Materialia, 2000. **48**(7): p. 1605-1615.
11. Nicolas, M. and A. Deschamps, *Characterisation and modelling of precipitate evolution in an Al–Zn–Mg alloy during non-isothermal heat treatments.* Acta Materialia, 2003. **51**(20): p. 6077-6094.
12. Deschamps, A. and Y. Bréchet, *Influence of quench and heating rates on the ageing response*

of an Al–Zn–Mg–(Zr) alloy. Materials Science and Engineering: A, 1998. **251**(1–2): p. 200-207.

13. Milkereit, B. and M.J. Starink, *Quench sensitivity of Al–Mg–Si alloys: A model for linear cooling and strengthening.* Materials & Design, 2015. **76**: p. 117-129.
14. Saunders, N., Guo, Z., Li, X., Miodownik, A.P., Schillé, J.P., *The calculation of TTT and CCT diagrams for general steels*, in *Internal report, Sente Software Ltd., U.K*. 2004.
15. Trzaska, J., A. Jagiełło, and L. Dobrzański, *The calculation of CCT diagrams for engineering steels.* Archives of Materials Science and Engineering, 2009. **39**(1): p. 13-20.
16. Colla, V., et al., *Prediction of Continuous Cooling Transformation Diagrams for Dual-Phase Steels from the Intercritical Region.* Metallurgical and Materials Transactions A, 2011. **42**(9): p. 2781-2793.
17. Du, Q., et al., *Microstructure evolution during homogenization of Al–Mn–Fe–Si alloys: Modeling and experimental results.* Acta Materialia, 2013. **61**(13): p. 4961-4973.
18. Jackson, A. and T. Sheppard, *Extrusion limit diagrams: effect of hmogenising conditions and extension to productivity analysis.* Materials Science and Technology, 1997. **13**(1): p. 61-68.
19. Clade, M.P. and T. Sheppard, *Extrusion limit diagrams containing structural and topological information for AA 6063 aluminium alloy.* Materials Science and Technology, 1993. **9**(4): p. 313-318.
20. Birol, Y., *The effect of homogenization practice on the microstructure of AA6063 billets.* Journal of Materials Processing Technology, 2004. **148**(2): p. 250-258.
21. Birol, Y., *Effect of cooling rate on precipitation during homogenization cooling in an excess silicon AlMgSi alloy.* Materials Characterization, 2012. **73**: p. 37-42.
22. Birol, Y., *Homogenization of EN AW 6005A Alloy for Improved Extrudability.* Metallurgical and Materials Transactions A, 2013. **44**(1): p. 504-511.
23. Birol, Y., *Optimization of homogenization for a low alloyed AlMgSi alloy.* Materials Characterization, 2013. **80**: p. 69-75.
24. Birol, Y., *Precipitation during homogenization cooling in AlMgSi alloys.* Transactions of Nonferrous Metals Society of China, 2013. **23**(7): p. 1875-1881.
25. Sun, Y., et al., *Effect of Mg2Si Phase on Extrusion of AA6005 Aluminum Alloy*, in *Light Metals 2014*. 2014, John Wiley & Sons, Inc. p. 429-433.

26. Priya, P., D.R. Johnson, and M.J.M. Krane, *Numerical Study of Microstructural Evolution During Homogenization of Al-Si-Mg-Fe-Mn Alloys.* Metallurgical and Materials Transactions A, 2016. **47**(9): p. 4625-4639.

27. Wen, Y.H., et al., *Phase-field modeling of bimodal particle size distributions during continuous cooling.* Acta Materialia, 2003. **51**(4): p. 1123-1132.

28. Radis, R., et al., *Multimodal size distributions of γ' precipitates during continuous cooling of UDIMET 720 Li.* Acta Materialia, 2009. **57**(19): p. 5739-5747.

29. Du, Q., et al., *Microstructural modeling of the homogenization heat treatment for AA3XXX alloys.* Jom, 2011. **63**(7): p. 35-39.

30. Du, Q., W.J. Poole, and M.A. Wells, *A mathematical model coupled to CALPHAD to predict precipitation kinetics for multicomponent aluminum alloys.* Acta Materialia, 2012. **60**(9): p. 3830-3839.

31. Holmedal, B., E. Osmundsen, and Q. Du, *Precipitation of Non-Spherical Particles in Aluminum Alloys Part I: Generalization of the Kampmann–Wagner Numerical Model.* Metallurgical and Materials Transactions A, 2016. **47**(1): p. 581-588.

32. Du, Q., et al., *Precipitation of Non-spherical Particles in Aluminum Alloys Part II: Numerical Simulation and Experimental Characterization During Aging Treatment of an Al-Mg-Si Alloy.* Metallurgical and Materials Transactions A, 2016. **47**(1): p. 589-599.

33. Du, Q., et al., *Modeling over-ageing in Al-Mg-Si alloys by a multi-phase CALPHAD-coupled Kampmann-Wagner Numerical model.* Acta Materialia, 2017. **122**: p. 178-186.

34. Scheil, E., Archiv Eisenhuttenwes, 1935. **8**: p. 565-567.

35. Tomellini, M., *Generalized additivity rule for the Kolmogorov–Johnson–Mehl–Avrami kinetics.* Journal of Materials Science, 2015. **50**(13): p. 4516-4525.

36. Liu, C.L., et al., *Microstructure evolution during homogenization of Al-Mg-Si-Mn-Fe alloys: Modelling and experimental results.* Transactions of Nonferrous Metals Society of China, 2017. **27**(4): p. 747-753.

37. Liu, C.L., et al., *The interaction between Mn and Fe on the precipitation of Mn/Fe dispersoids in Al-Mg-Si-Mn-Fe alloys.* Scripta Materialia, 2018. **152**: p. 59-63.

38. Kozeschnik, E., I. Holzer, and B. Sonderegger, *On the Potential for Improving Equilibrium Thermodynamic Databases with Kinetic Simulations.* Journal of Phase Equilibria and

Diffusion, 2007. **28**(1): p. 64-71.

39. Povoden-Karadeniz, E., et al., *CALPHAD modeling of metastable phases in the Al–Mg–Si system.* Calphad, 2013. **43**(0): p. 94-104.

40. Du, Y., et al., *Diffusion coefficients of some solutes in fcc and liquid Al: critical evaluation and correlation.* Materials Science and Engineering a-Structural Materials Properties Microstructure and Processing, 2003. **363**(1-2): p. 140-151.

41. Hatch, J.E., A. Association, and A.S. Metals, *Aluminum: Properties and Physical Metallurgy*. 1984: American Society for Metals.

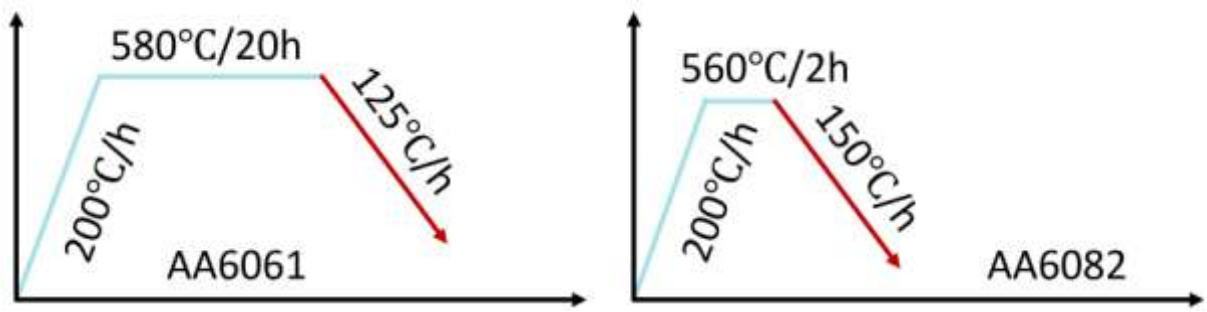

Fig. 1 Schematic of the thermal history used for the homogenization heat treatment. The heating rate is 200^{0}C/h from room temperature to the soaking temperature. The soaking time is 20 and 2 hours respectively. The cooling rate is 125 ^{0}C/h and 150 ^{0}C/h respectively. The samples are taken out of the furnace at the end of soaking, 550 ℃, 500 ℃, 450 ℃,400 ℃, 350 ℃, 300 ℃, 250 ℃, 200℃ for quenching in water.

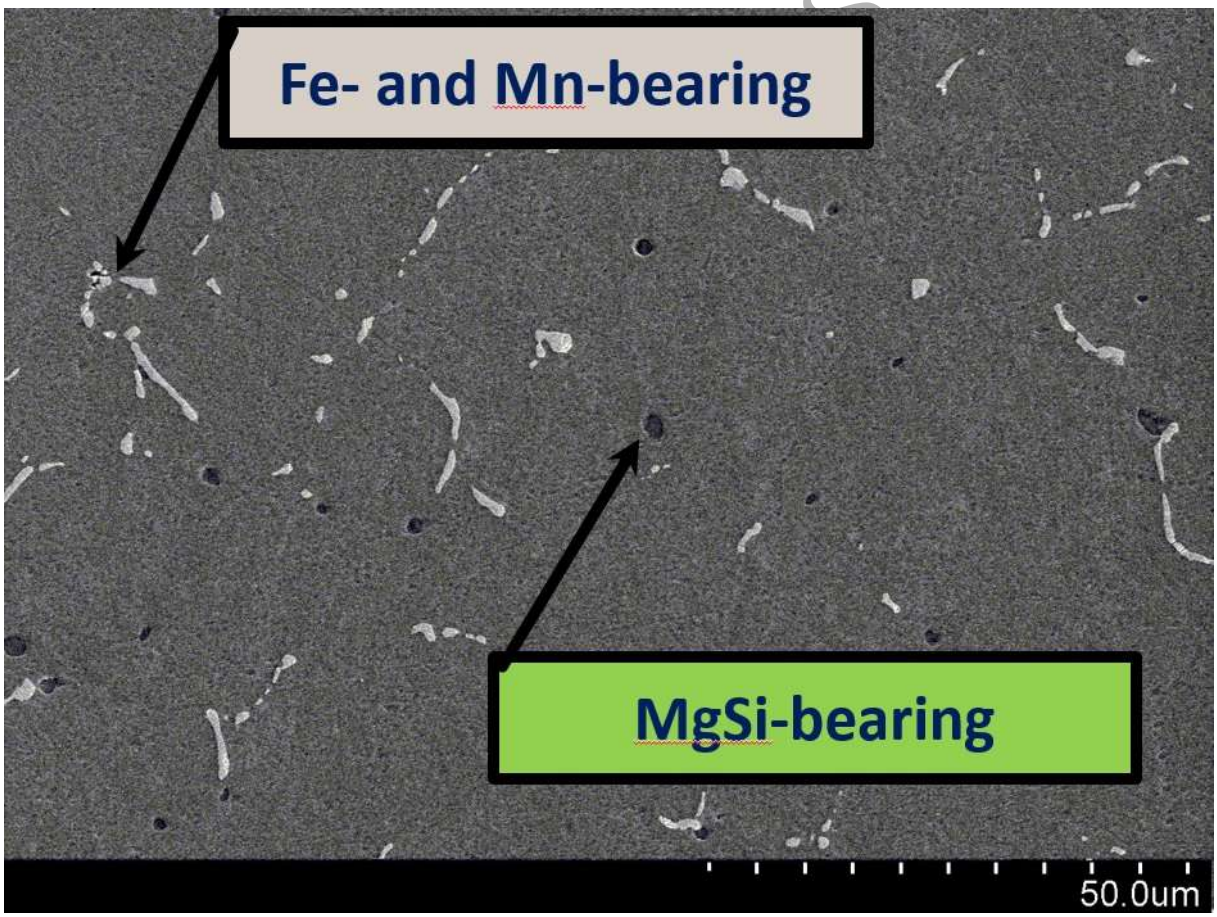

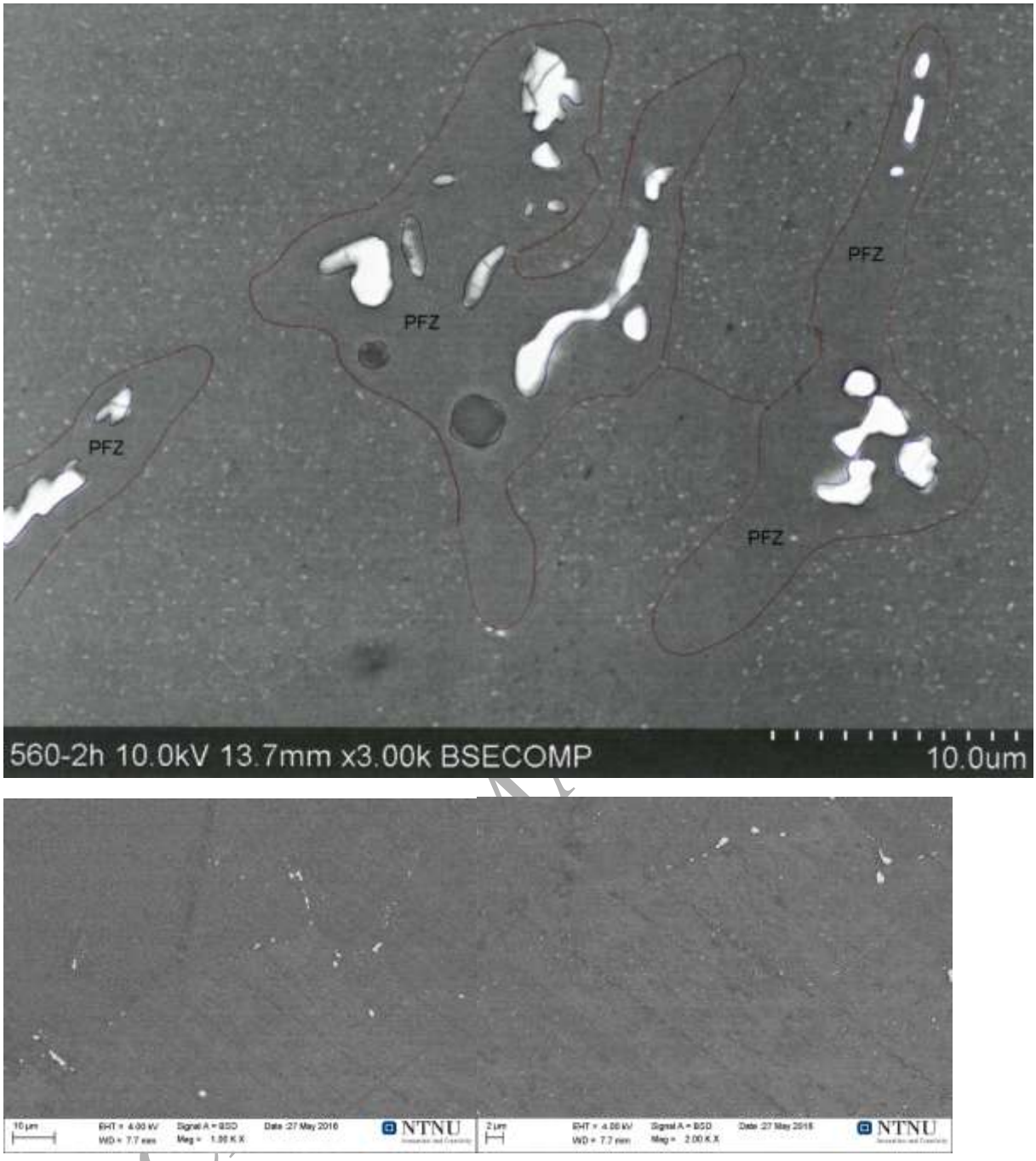

Fig. 2 The SEM images revealing the microstructural state of the AA6082 alloy (a, b) and the AA6061 (c) (d) after soaking treatment.

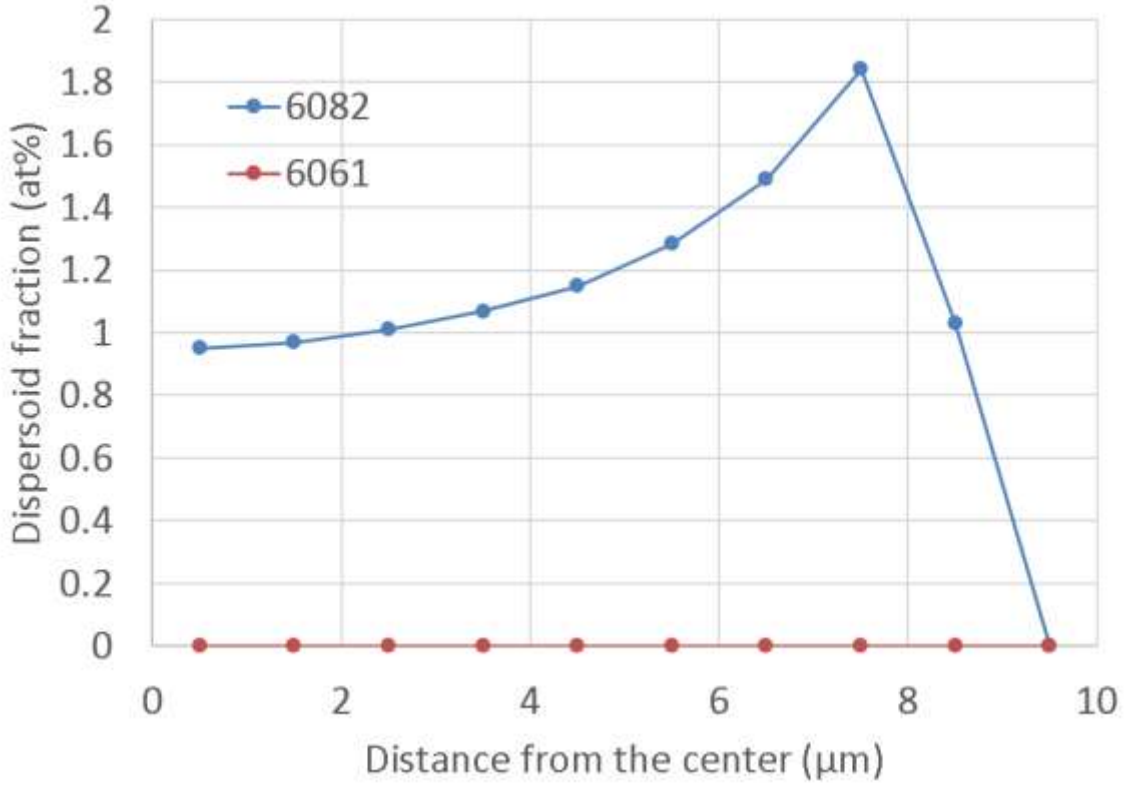

Fig. 3 The predicted profiles of disperoids fractions along an average dendrite arm for the AA6082 and AA6061 alloys

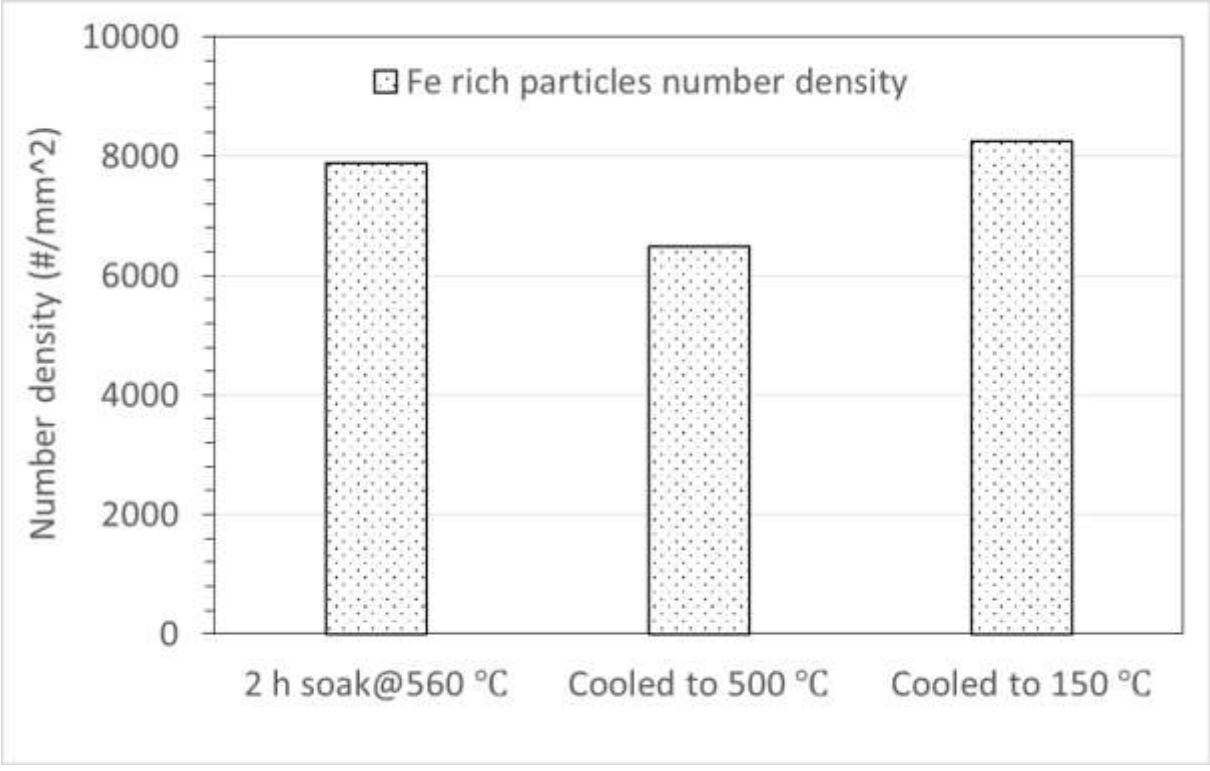

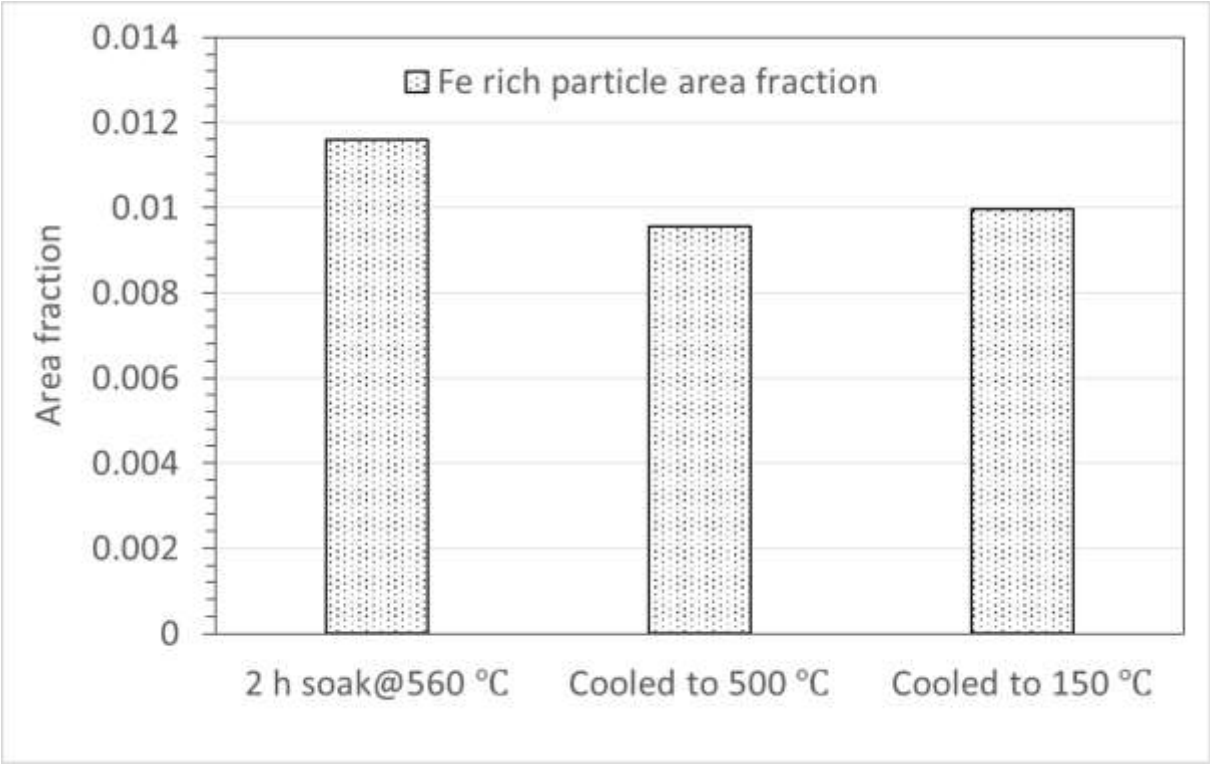
Fe rich particle area fraction
Area fraction
0.014
0.012
0.01
0.008
0.006
0.004
0.002
0
2 h soak@560 °C
Cooled to 500 °C
Cooled to 150 °C

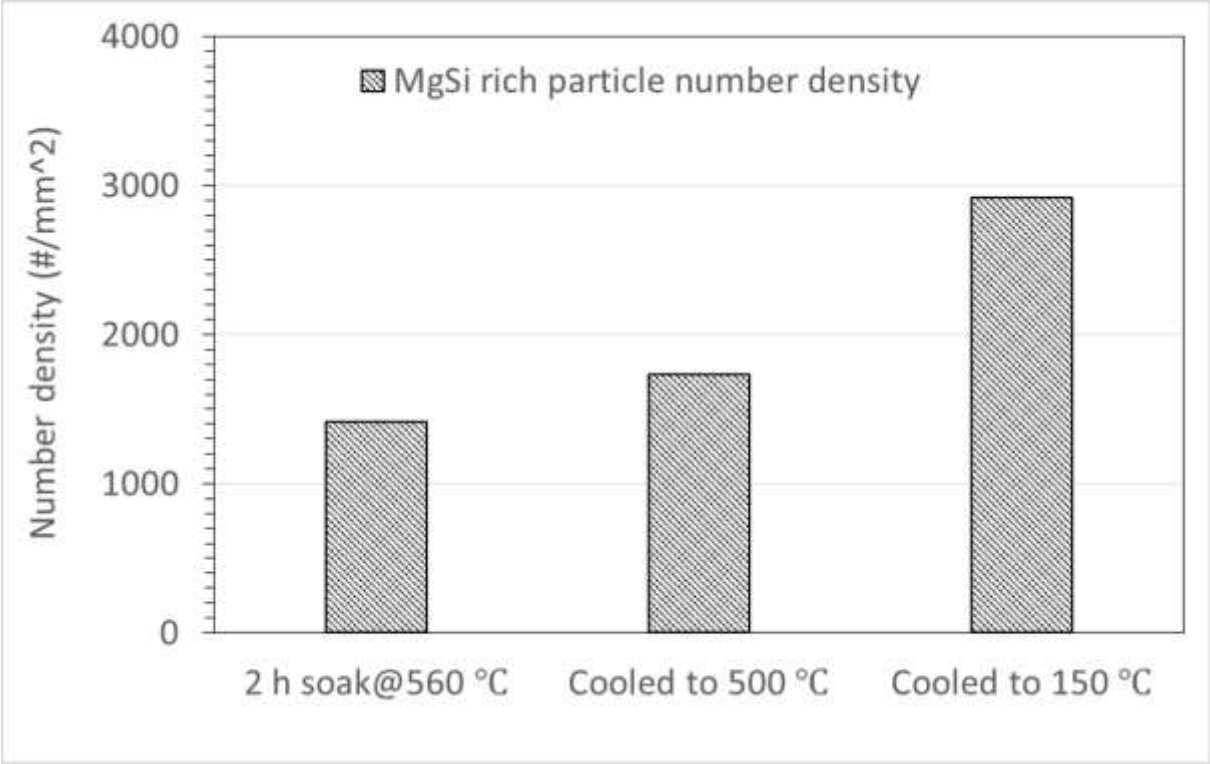
MgSi rich particle number density
Number density (#/mm^2)
4000
3000
2000
1000
0
2 h soak@560 °C
Cooled to 500 °C
Cooled to 150 °C

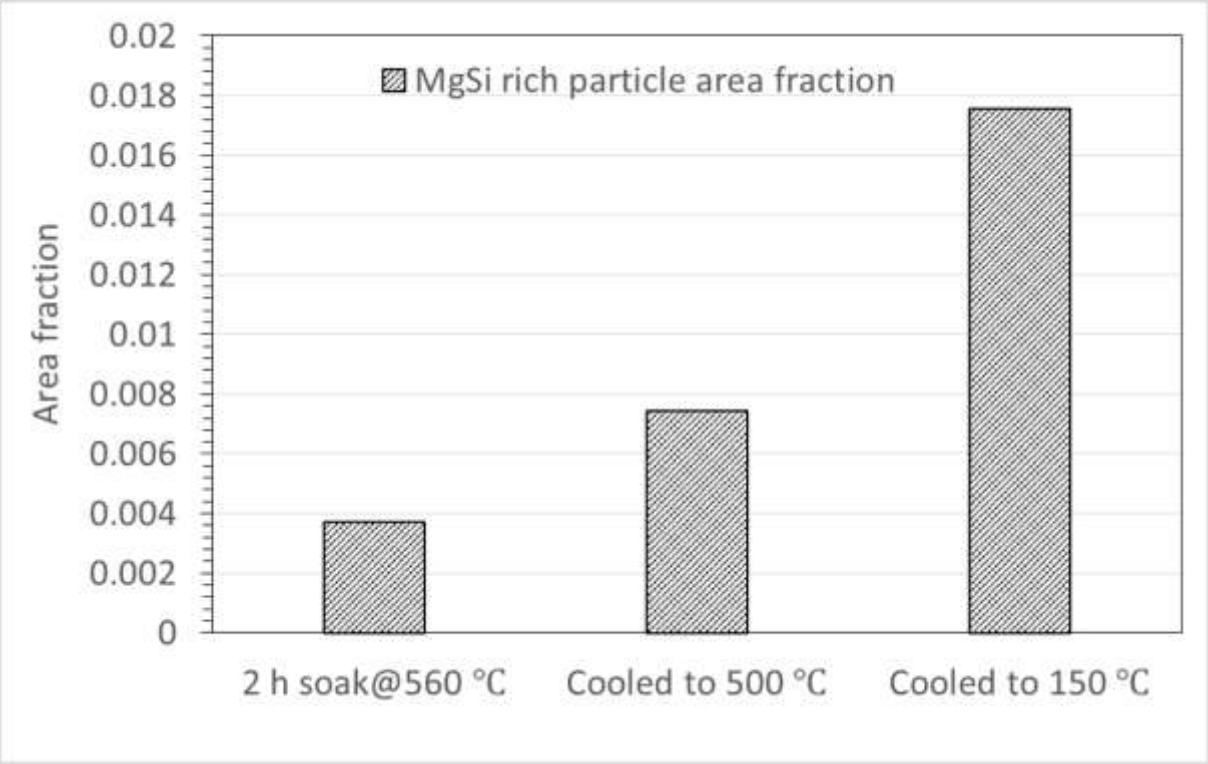

Fig. 4 The measured interdendritic particles fractions at the start of cooling, middle and end of cooling of the AA6082 alloy.

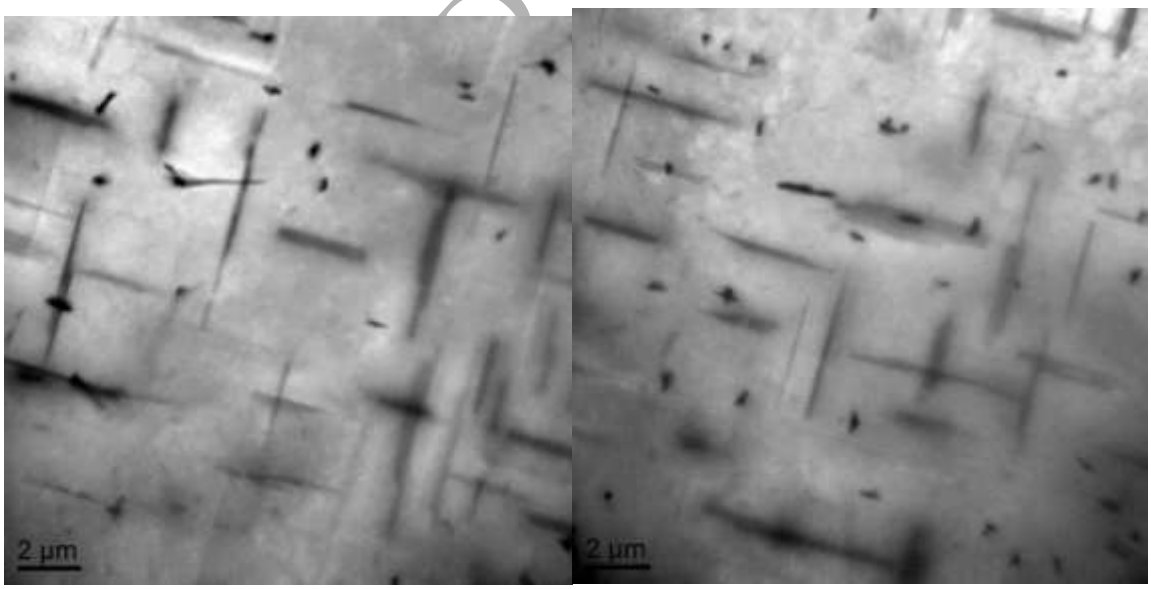

Fig. 5 Two TEM images taken at the end of the cooling of the AA6061 alloys.

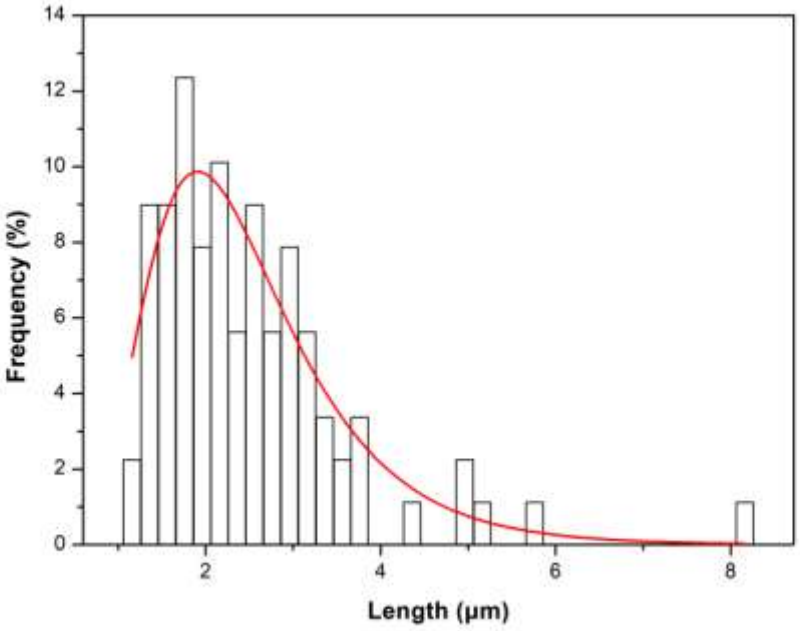
Frequency (%)
Length (μm)
0
2
4
6
8
10
12
14

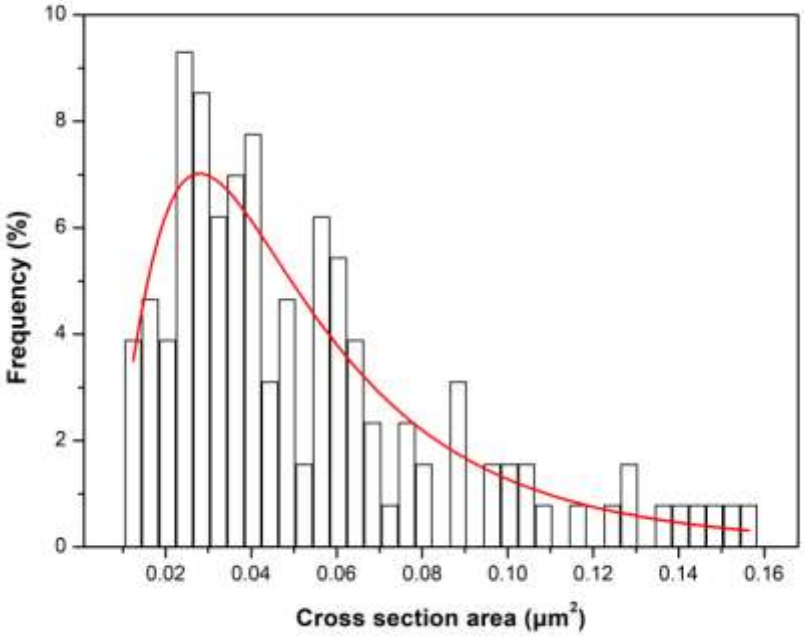
Frequency (%)
Cross section area (μm²)
0
2
4
6
8
10
0.02
0.04
0.06
0.08
0.10
0.12
0.14
0.16

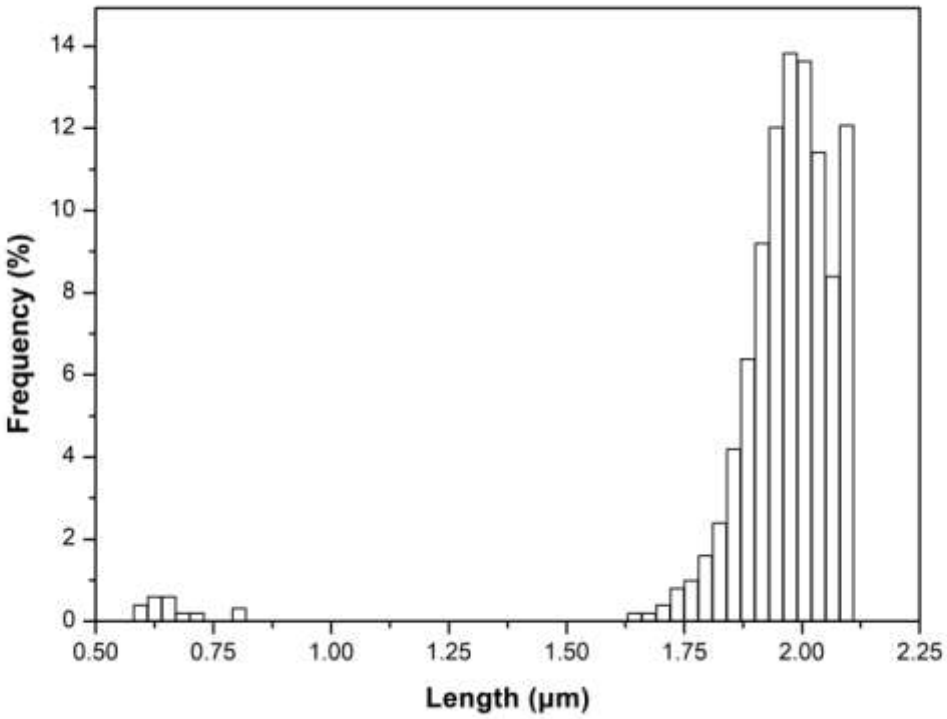

Fig. 6 The measured (a) cross area and (b) length and predicted (c) length distributions of MgSi particles obtained at the end of cooling of the AA6061 alloy

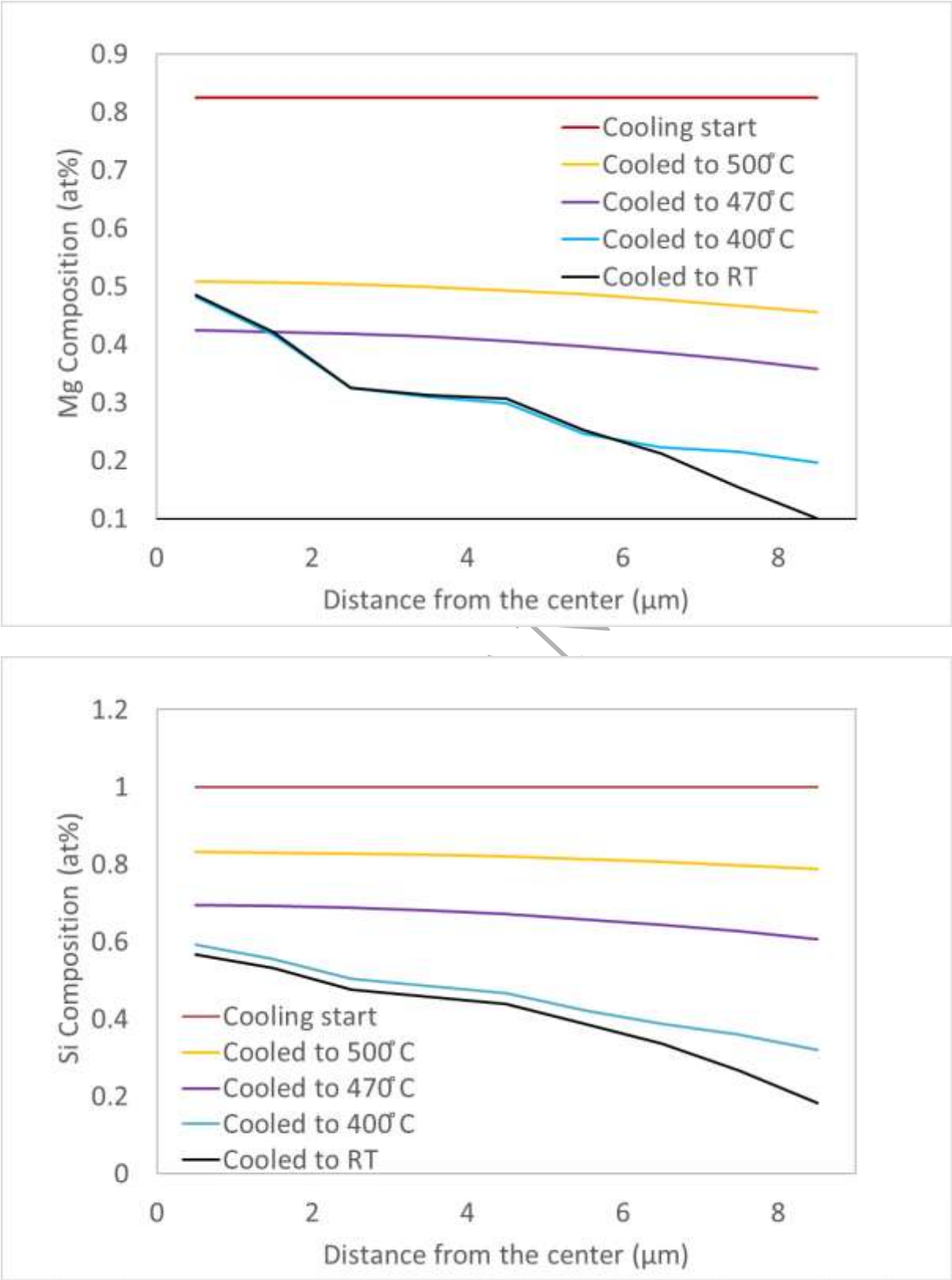

Fig. 7 the average composition profiles of (a) Mg and (b) Si at the start, middle and end of the cooling.

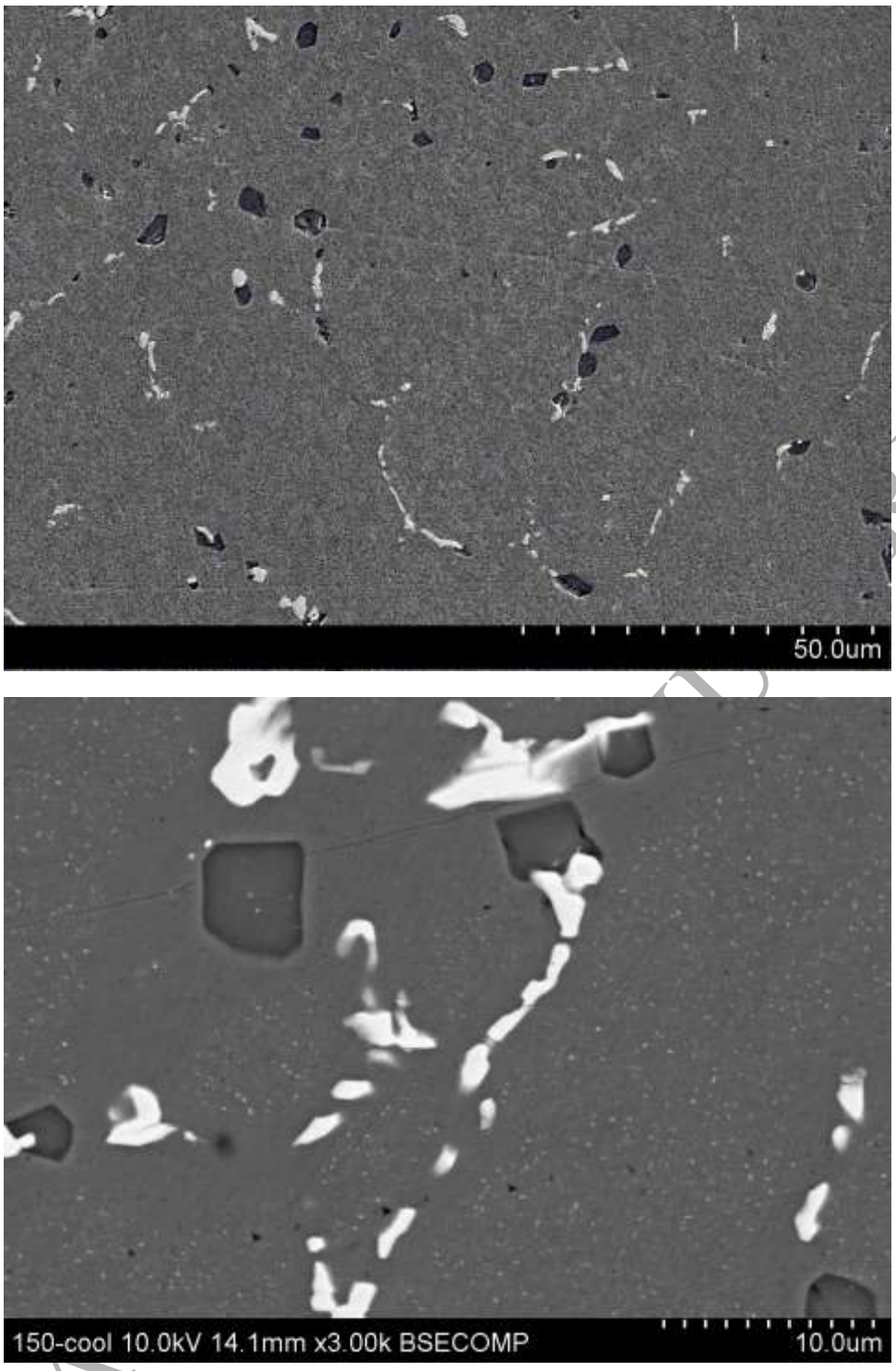

Fig. 8 The SEM images taken at the end of the cooling of the AA6082 alloys.

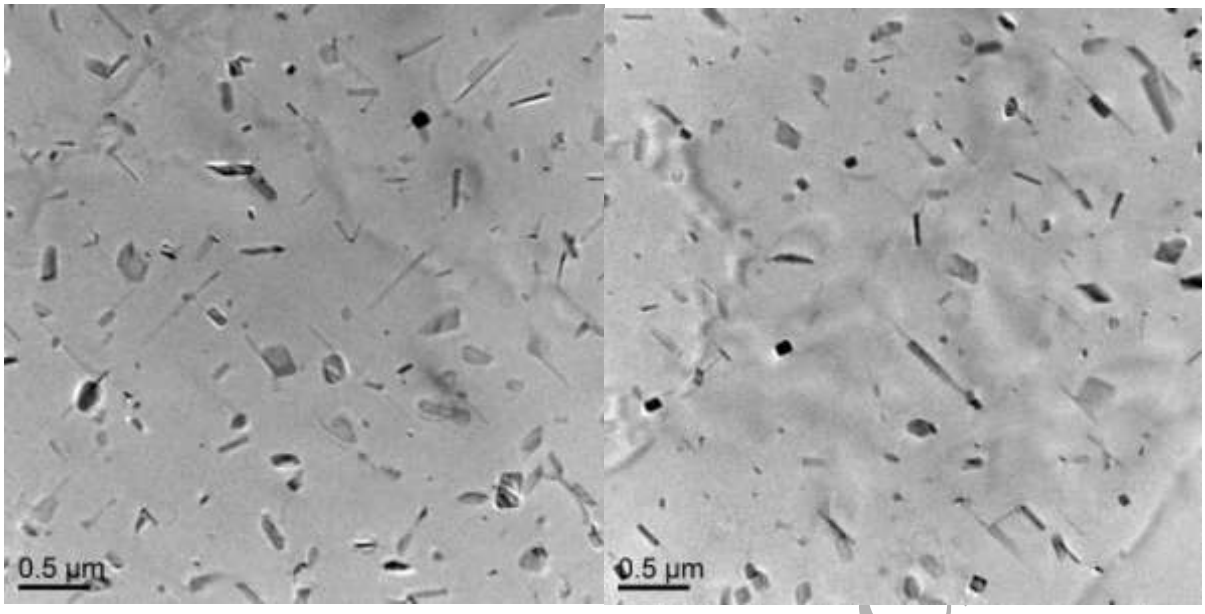

Fig. 9 The TEM images taken at the end of the cooling of the AA6082 alloys.

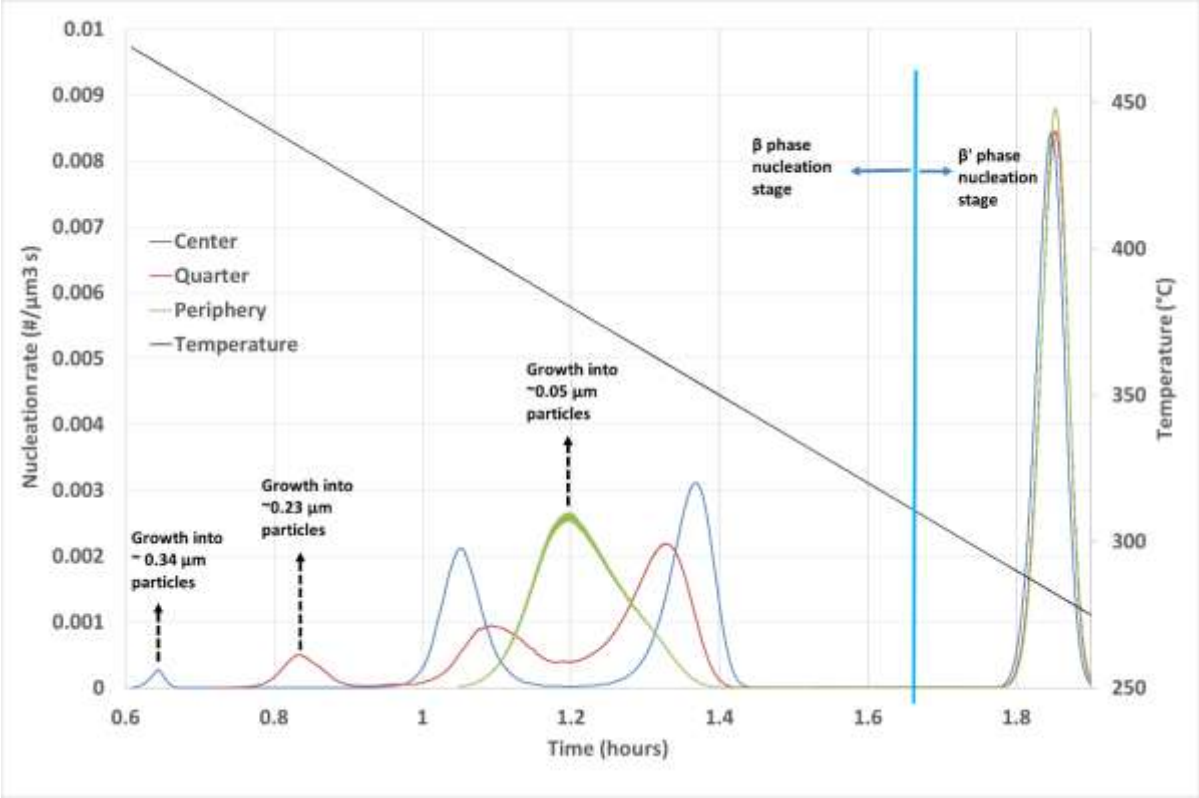

Fig. 10 The predicted nucleation rates at the different locations of a dendrite arm (periphery, 1 quarter from the periphery and centre) during the cooling of the AA6082 alloy.

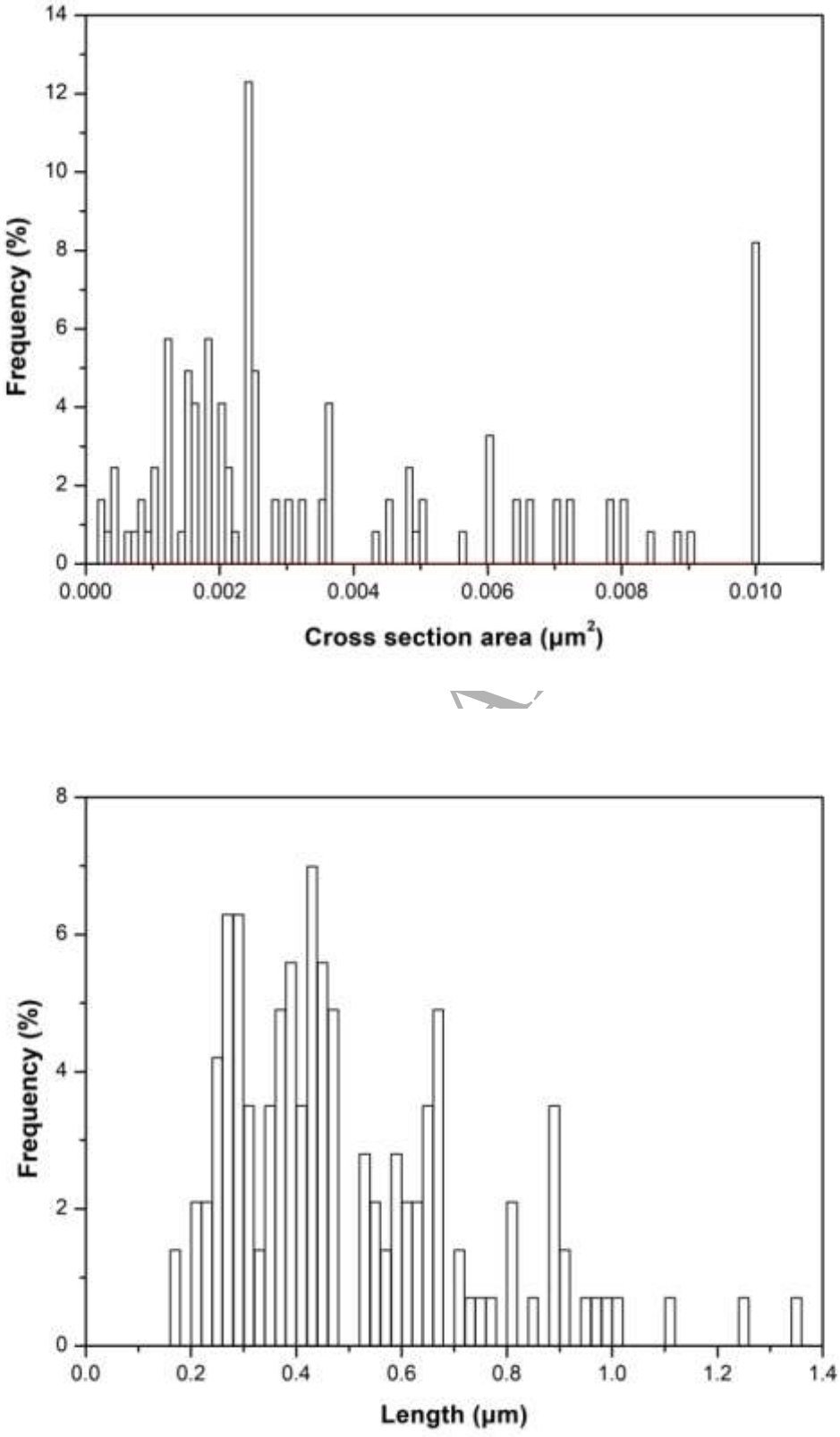

Fig. 11 The measured Mg-Si particles cross section area (a) and length (b) distributions obtained at the end of cooling of the AA6082 alloy.

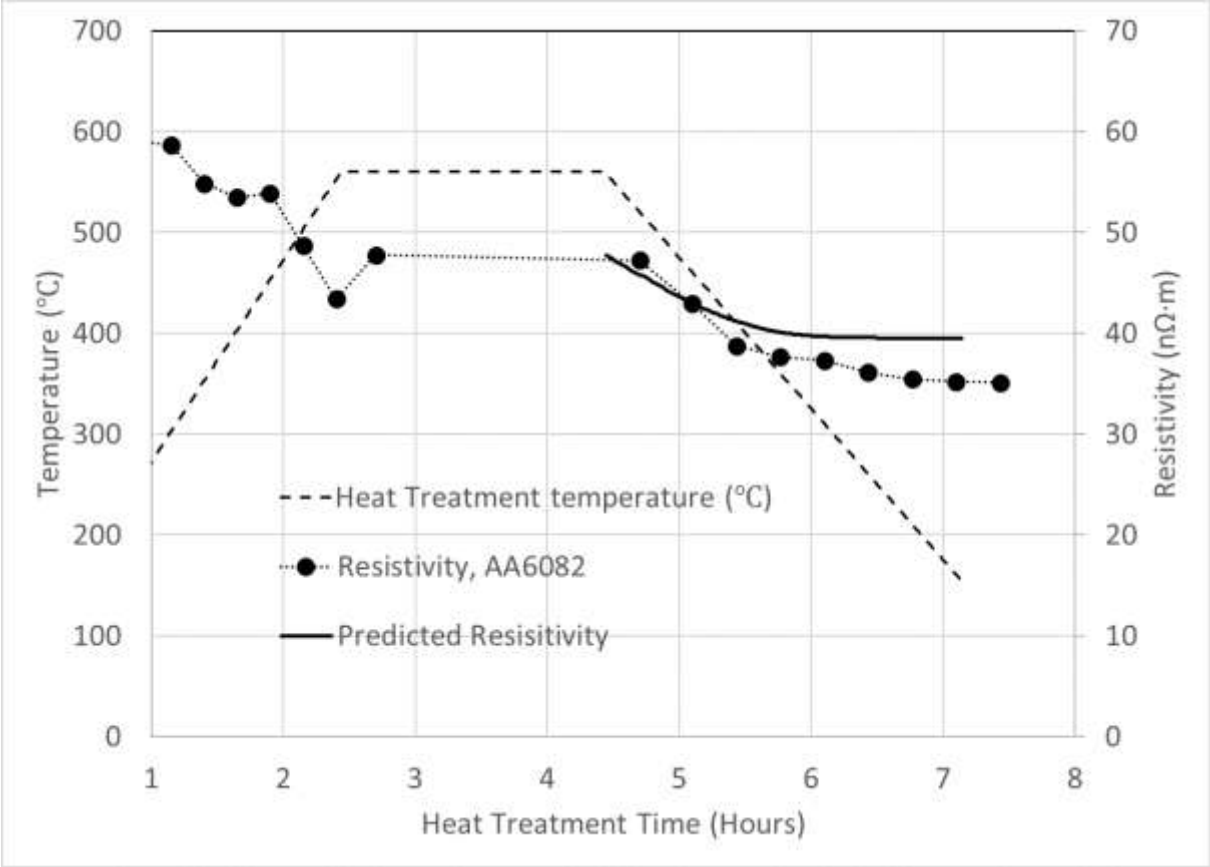

Fig. 12 The measured and predicted resistivity evolution during the cooling of the AA6082 alloy

Table 1 Interfacial energies used in the simulations and calculated using Kozeschnik's solution enthalpy method

Interface with FCC phase	Used in the simulations	Calculated using Kozeschnik's solution enthalpy, averaging in {100}, {111} and {110} planes
β'	0.09	0.198
B	0.12	0.227

Table 2 Other material property and nucleation input parameters used in the simulations

Molar volume of β, β' and FCC phases		1.0×10^{-5} m^3/mol	
Lattice parameters in FCC phase		0.404 nm	
Diffusivities in the FCC phase [40]		Diffusion constant (m^2/s)	activation energy (kJ/mole)
	Mg	1.49×10^{-5}	120.5
	Si	1.38×10^{-5}	117.6
Gibbs-Thomson phase diagram		Metastable phase diagram generated by first principle calculations in [39].	

Table 3 Chemistry of the two alloys investigated in the current work

Alloy	Mg (wt%)	Si (wt%)	Fe (wt%)	Mn (wt%)	Cu (wt%)
AA6082	1.08	1.23	0.27	0.62	0.08
AA6061	0.8085	0.4935	0.0089	0.1365	0.7057

Table 4. The predicted solid solution levels and constituent particles fractions at the end of soaking treatment

	Solid solution solute level (wt%)				Constituent particles fraction (%)	
	Mg	Si	Fe	Mn	Fe/Mn particles	Mg2Si
AA6082	0.85	0.88	0.0018	0.13	1.07	0.43
AA6061	0.81	0.49	0.0045	0.13	0.03	0

Table 5. The predicted and measured intragranular MgSi particles and Mg_2Si constituent particles fractions at the end of cooling of the AA6082 alloy

	Intragranular MgSi particles fraction (%)	Mg_2Si Constituent particles fraction (%)
Prediction	0.29	1.7
Measurement	0.47±0.13	1.78±0.5

Graphical abstract

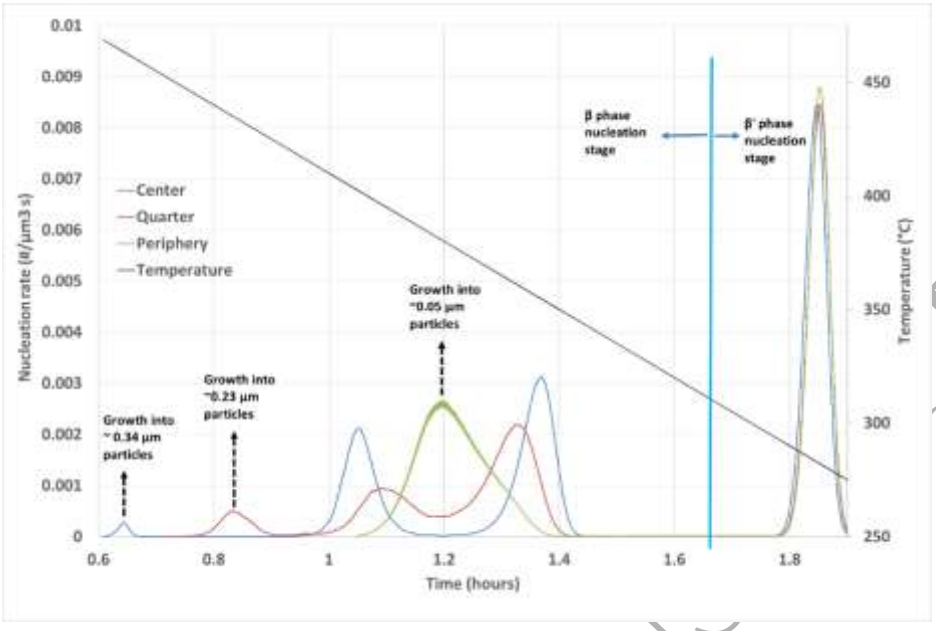

Fig. 1 The predicted nucleation rates at the different locations of a dendrite arm (periphery, 1 quarter from the periphery and centre) during the cooling of the AA6082 alloy.

The proposed model reveals that multi nucleation peaks arise because of:

1. the existences of local microchemistry variations along a dendrite arm
2. the continuous cooling enables the build-up of sufficient thermodynamic nucleation driving forces.

The complex nucleation behaviour shown in this figure is useful in interpreting the multi-modal particles distribution curves from the TEM measurements shown in the following figures.

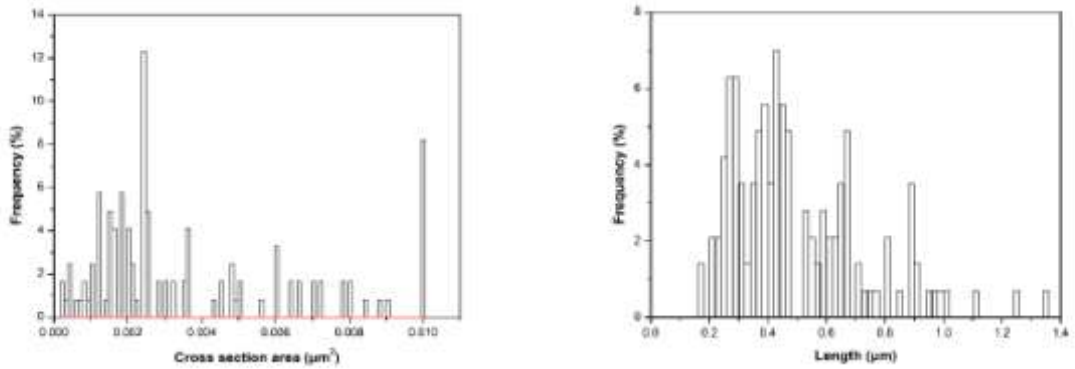

(a)

(b)

Fig. 2 The measured Mg-Si particles cross section area (a) and length (b) distributions obtained at the end of cooling of the AA6082 alloy.